Asymmetry of spin-flip of polarized protons in the inelastic scattering to the first 2^+ states of ^{48}Ti and ^{50}Ti

M. Tomizawa, T. Aoki, Y. Aoki, T. Murayama,* T. Sakai, Y. Tagishi, and K. Yagi
Institute of Physics and Tandem Accelerator Center, University of Tsukuba, Tsukuba, Ibaraki 305, Japan
(Received 2 October 1989)

Angular distributions of the differential cross section, analyzing power, spin-flip probability, and spin-flip asymmetry in the excitation of the first 2^+ states in ^{48}Ti and ^{50}Ti were measured at incident energies of 11 and 18 MeV using the $(p,p'\gamma)$ coincidence technique with a polarized proton beam. The angular distributions show strong incident energy and target dependence. The results were analyzed in terms of a macroscopic coupled-channels method based on the vibrational model and of the microscopic distorted wave Born approximation based on shell-model wave functions and effective nucleon-nucleon interactions. The spin-flip asymmetry is quite sensitive to the spin-dependent part in the interaction that causes inelastic scattering.

I. INTRODUCTION

A large number of measurements have been done to investigate the spin dependence of the interaction which causes the proton inelastic scattering from even-even nuclei leading to the first 2^+ state. These measurements have been classified into the two types: measurements of the analyzing power of the reaction using a polarized proton beam[1] and measurements of the spin-flip probability using the $(p,p'\gamma)$ method developed by Schmit *et al.*[2] These experimental results have been analyzed in terms of the macroscopic and microscopic models, but the spin dependences of the inelastic interaction are not yet well understood. Some measurements of spin-flip protons with the polarized beam have been done,[3-5] but they were not to study the direct reaction mechanism. Here we present the first measurement and analysis that applied asymmetry of spin-flip of polarized protons to the direct reaction process.

This paper covers four independent observables in the proton inelastic scattering: that is, differential cross section $\sigma(\theta)$, analyzing power $A_y(\theta)$, polarization $P_y(\theta)$, and spin-flip probability $S(\theta)$. These observables are defined as follows:

$$\sigma(\theta)=\tfrac{1}{2}[\sigma_{++}(\theta)+\sigma_{+-}(\theta)+\sigma_{--}(\theta)+\sigma_{-+}(\theta)] , \quad (1)$$

$$A_y(\theta)=\tfrac{1}{2}\{[\sigma_{++}(\theta)+\sigma_{+-}(\theta)] -[\sigma_{--}(\theta)+\sigma_{-+}(\theta)]\}/\sigma(\theta) , \quad (2)$$

$$P_y(\theta)=\tfrac{1}{2}\{[\sigma_{++}(\theta)+\sigma_{-+}(\theta)] -[\sigma_{--}(\theta)+\sigma_{+-}(\theta)]\}/\sigma(\theta) , \quad (3)$$

and

$$S(\theta)=\tfrac{1}{2}[\sigma_{+-}(\theta)+\sigma_{-+}(\theta)]/\sigma(\theta) , \quad (4)$$

where the σ_{+-}, e.g., is the differential cross section from an initial state with the spin projection $+\frac{1}{2}$ of the incident proton to a final state with the spin projection $-\frac{1}{2}$ of the outgoing proton on the z axis, which is chosen along the normal to the scattering plane. In general these observables are sensitive to the spin-dependent term in the optical potential. It was shown by Satchler[6] that the difference $A_y(\theta)-P_y(\theta)$ in a direct inelastic scattering of nucleons arises from the interference between the spin-independent and spin-dependent interactions in the adiabatic approximation if the time-reversal-invariant and parity-conservation laws hold.[7] Therefore it is expected that $A_y(\theta)-P_y(\theta)$ is sensitive to the spin-dependent part in the interaction which causes the inelastic scattering. Measurement of $P_y(\theta)$ is very difficult because it requires a double scattering experiment. Instead of $P_y(\theta)$ we have measured a spin-flip asymmetry $\epsilon(\theta)$ which is defined as

$$\epsilon(\theta)=\frac{\sigma_{+-}(\theta)-\sigma_{-+}(\theta)}{\sigma_{+-}(\theta)+\sigma_{-+}(\theta)} , \quad (5)$$

by using a polarized proton beam. Furthermore when we decompose the partial cross section $\sigma_{m_i m_f}$ into

$$\sigma_{m_i m_f}=\sigma^{(0)}_{m_i m_f}+\sigma^{(1)}_{m_i m_f}+\sigma^{(\mathrm{int})}_{m_i m_f} , \quad (6)$$

the spin-flip asymmetry is written as[8]

$$\epsilon=\frac{\sigma^{(\mathrm{int})}_{+-}-\sigma^{(\mathrm{int})}_{-+}}{\sigma^{(0)}_{+-}+\sigma^{(1)}_{+-}+\sigma^{(0)}_{-+}+\sigma^{(1)}_{-+}} , \quad (7)$$

where the $\sigma^{(0)}_{m_i m_f}$ ($\sigma^{(1)}_{m_i m_f}$) term is the contribution to the partial cross section only from the spin-independent (-dependent) interaction, and $\sigma^{(\mathrm{int})}_{m_i m_f}$ is the interference term between the spin-independent and -dependent parts. Thus spin-flip asymmetry $\epsilon(\theta)$ also arises from the interference between the spin-independent and -dependent interactions as the difference $A_y(\theta)-P_y(\theta)$ does. Moreover, the spin-flip asymmetry $\epsilon(\theta)$ should be more sensitive to the spin-dependent interaction than $A_y(\theta)-P_y(\theta)$. This is because the denominator of $\epsilon(\theta)$ is smaller than that of $A_y(\theta)-P_y(\theta)$, where the difference between analyzing power and polarization is written as $A_y(\theta)-P_y(\theta)=[\sigma_{+-}(\theta)-\sigma_{-+}(\theta)]/\sigma(\theta)$.

We have measured $\sigma(\theta)$, $A_y(\theta)$, $S(\theta)$, and $\epsilon(\theta)$ for inelastic scattering from ^{48}Ti and ^{50}Ti leading to ^{48}Ti(2^+_1,0.99 MeV) and ^{50}Ti(2^+_1,1.55 MeV) at $E_p=11$

and 18 MeV using the $(p,p'\gamma)$ coincidence method with the polarized proton beam. The reasons why the target nuclei ^{48}Ti and ^{50}Ti were chosen are the following.

(1) From a microscopic viewpoint on nuclear structure and nuclear interaction: The nucleus ^{50}Ti($Z=22$, $N=28$) has two protons outside the $Z=20$ closed shell and the $N=28$ closed shell, while the nucleus ^{48}Ti($Z=22$, $N=26$) is a two-proton particle and two-neutron hole nucleus. Thus we expect to have good shell-model wave functions of the nuclei based on the shells of $f_{7/2}$, $f_{5/2}$, $p_{3/2}$, and $p_{1/2}$. On the basis of these microscopic nuclear-structure wave functions, we can expect to extract the effective nucleon-nucleon interaction in the inelastic scattering process.

(2) From a macroscopic viewpoint: In the excitation of the first 2^+ state, ^{48}Ti shows much more collective nature in quadrupole surface vibration than ^{50}Ti. Indeed the quadrupole deformation parameter β_2 for ^{48}Ti (^{50}Ti) is $\beta_2=0.265$ (0.175). Thus the excitation of the first 2^+ states in the two nuclei is expected to involve very different coupling between spin and collective degrees of freedom.

II. EXPERIMENTAL PROCEDURE

The polarized proton beam was produced by a Lamb-shift-type polarized ion source with a spin filter at the Tandem Accelerator Center, University of Tsukuba (UTTAC).[9] The magnetic substate of protons was interchanged by a magnetic field reversal of the spin filter and the argon areas. They were controlled by external signals from a Fast Spin State Interchange Control System (FASSICS).[10] The spin states are usually interchanged every few seconds corresponding to the preset counts of a digitized beam current integration. The dead time is about several hundreds of msec, which is sufficient to complete interchanging of the spin states.

The ^{50}Ti target obtained from the Oak Ridge National Laboratory was a self-supporting metallic foil with thickness of 900 μg/cm^2, enriched to 68% in ^{50}Ti, and 24% in ^{48}Ti. The inelastically scattered protons from the first excited states of ^{48}Ti(0.99 MeV) and ^{50}Ti(1.55 MeV) were well separated from the difference of these energies. The contamination of carbon and oxygen in the present target is estimated to be 37 μg/cm^2 and 16 μg/cm^2, respectively, which causes a large background for the measurement of the inelastic scattering from ^{48}Ti or ^{50}Ti over a certain angular region. The effect of the contaminant was eliminated by measuring the cross sections and analyzing powers for elastic scattering from carbon and oxygen by use of a mylar target.

Measurements were carried out in a large scattering chamber, 90 cm in diameter and 45 cm in height (Fig. 1). The chamber contains a turntable and a turnarm on which particle detectors were mounted. The scattered protons were detected by two or three pairs of solid state detectors which were placed on both sides of the beam direction at 20° or 30° intervals. The lithium-drifted Si solid detectors having 3.0 and 3.5 mm thickness were used for the incident energies of 11 and 18 MeV, respectively. The typical solid angle of the detectors was 8 msr, corresponding to an angular acceptance of $\Delta\theta=\pm3°$. The γ rays emitted vertically were detected with a NaI(Tl) crystal, 76 mm × 76 mm, mounted on a photomultiplier tube (Fig. 1). The detector was placed at 9 cm above the target and separated from vacuum. Deexcited γ rays were collimated by a defining lead slit of 5 cm thickness, which has a conical aperture. The half-angle subtended by the midplane of the γ detector was about 10°, corresponding to a solid angle of 100 msr. In order to reduce the γ-ray background the detector was surrounded by 10-cm-thick lead blocks placed on the table in the chamber. In addition the Faraday cup was shielded with lead bricks and was placed at a distance of about 4 m from the target.

The absolute efficiency of the γ-ray detector was determined by using calibrated standard sources. The obtained detector efficiencies of a full energy peak were 27% for 0.99-MeV γ rays and 18% for 1.55-MeV γ rays corresponding to the first excited energies of ^{48}Ti and ^{50}Ti, respectively. The uncertainty of the absolute values of these efficiencies is estimated to be within 15%.

The drift of the beam position on the target causes a serious false asymmetry for the measurements. In the case of the incident energy of 11 MeV, the incident beam was well collimated with a double-slit system by lead

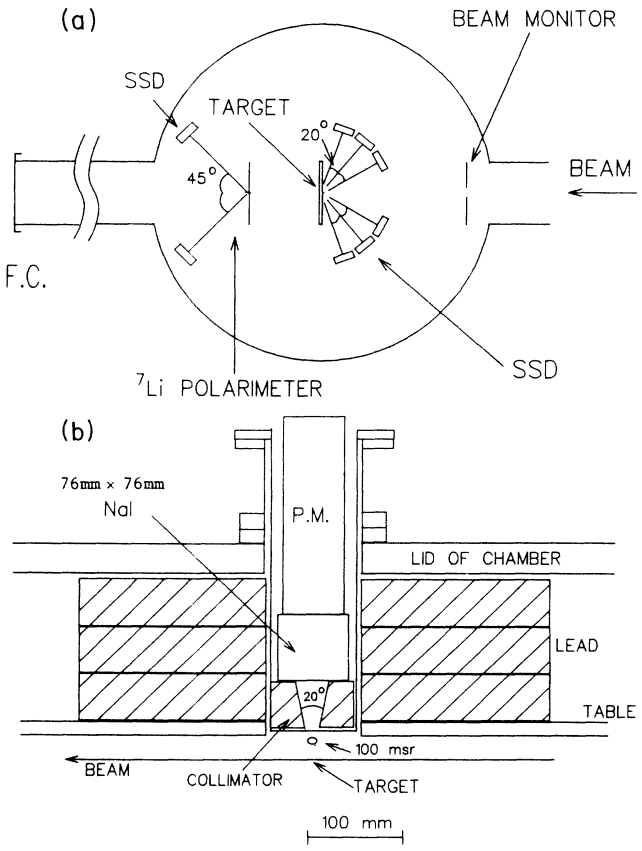

FIG. 1. Schematic views of the experimental arrangement in the scattering chamber (a) and the γ-ray detector system (b).

blocks which reduced the γ-ray background from the slit. When the bombarding energy was increased to 18 MeV, we were not able to use the slit system, because the γ-ray background from the beam-defining slits increased extremely. Instead of using such a slit system, we monitored the beam position by using the real-time beam-position monitoring system. A 15-μm-thick aluminum foil with a circular hole of radius 1 mm was placed 50 cm upstream from the target. Since the beam spot size is less than about 1 mm in radius at the target position, most incident protons pass through the hole. When the beam direction is shifted, the scattered particles from the hole edge can be detected by a solid-state detector placed at 90° with respect to the beam line in the vertical plane, and then the data-taking is stopped. The beam position can be monitored within drift of 1 mm by using this system.

A beam polarimeter based on the p-^{4}He elastic scattering has been usually used. However, in the present experiment this polarimeter cannot be used because of the γ-ray background from the entrance and exit windows of the ^{4}He gas target. Thus a proton polarimeter based on the ^{7}Li$(\vec{p},\alpha)^4$He reaction was used. This reaction has a large analyzing power at $\theta_{\rm lab}=45°$ ($A_y=0.949\pm0.004$ and 0.890 ± 0.005 at $E_p=11$ and 18 MeV, respectively).[11] The polarimeter was placed 30 cm downstream from the target; see Fig. 1. Scattered alpha particles were detected by a pair of solid state detectors which was placed at $\theta_{\rm lab}=45°$ on each opposite side of the incident beam. The absolute value of the beam polarization was then measured within an accuracy of $\pm2\%$.

A block diagram of the electronics system is shown in Fig. 2. The fast-timing signals were generated by constant-fraction discriminators (CFD's) following timing filter amplifiers (TFA's). The outputs of the constant-fraction discriminators coming from each of the particle detectors were mixed and then they provided each start pulse for a time-to-amplitude converter (TAC). A stop pulse was provided by a signal from the γ-ray detector. The single energy spectra of the six particle detectors were taken by using three multichannel pulse-height analyzers (MCA's). The data-taking system based on VAX-750 and VAX-780 computers was used.

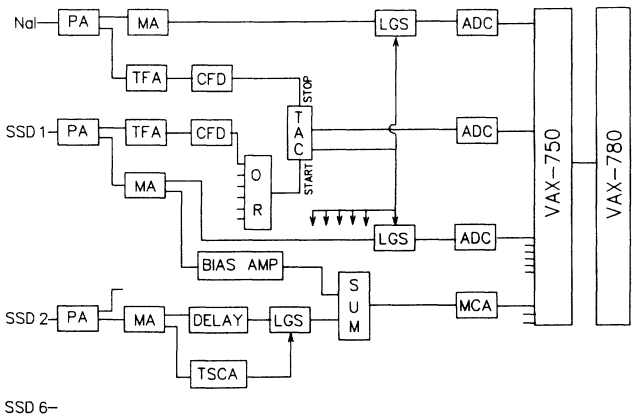

FIG. 2. Schematic diagram of the electronics.

III. EXPERIMENTAL RESULTS

Data were stored as a triple-parameter data record: the energy signals of the coincident particles and γ rays, and the TAC signals. The typical resolution was 3 nsec (FWHM) and the signal-to-noise ratio was about 20/1. Figure 3 shows γ-ray spectra which were obtained by setting the windows around the true peak of the TAC spectrum and the inelastic peaks of ^{48}Ti and ^{50}Ti. The proton spectrum gated by the true peak of the TAC is shown in Fig. 4, together with chance coincident spectrum of protons. Typical beam intensity on the target was suppressed to 30 nA so as to keep the counting rate of the γ-ray detector less than 3×10^4 per sec. The typical beam polarization was 85%. We needed nine days for each of the experiments of $E_p=11$ and 18 MeV. The true coincidence rate was 10–20 counts per hour.

Measured angular distributions of differential cross section $\sigma(\theta)$, analyzing power $A_y(\theta)$, spin-flip probability $S(\theta)$, and spin-flip asymmetry $\epsilon(\theta)$ are shown in Fig. 5. The error bars represent statistical errors only. The partial differential cross sections are shown in Fig. 6. We corrected the effect arising from deexcitation γ rays from other magnetic substates of the 2_1^+ excited nuclei ($m=0\rightarrow0$ and $m=\pm2\rightarrow0$), which is caused by the finite solid angle of the actual γ-ray detector. We estimated that the maximum value of the error caused by this effect was less than the statistical errors except for the forward

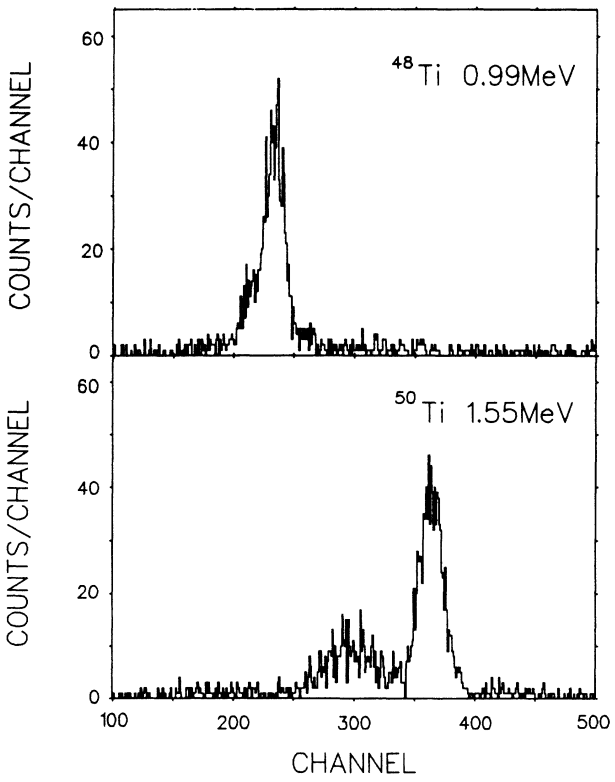

FIG. 3. Coincident γ-ray spectra. The upper peak is the full energy peak for deexcitation γ-rays from 2_1^+ of ^{48}Ti and the lower peak is that from 2_1^+ of ^{50}Ti.

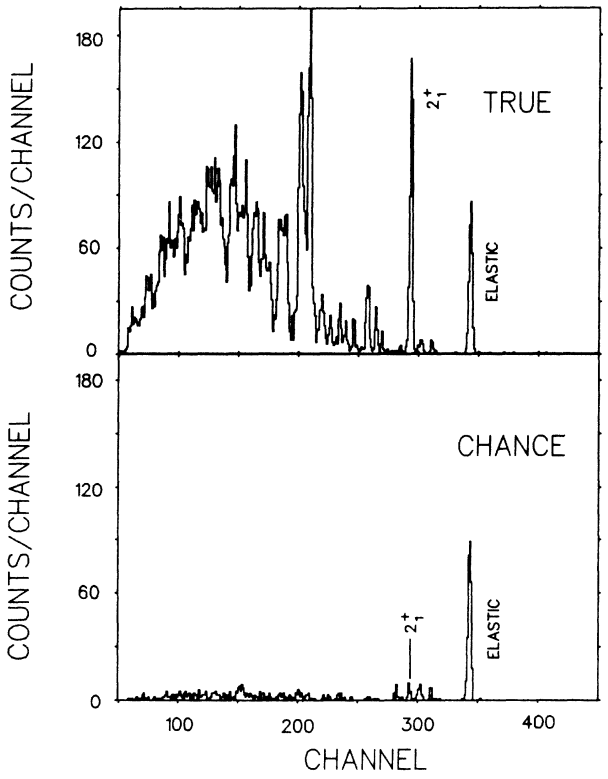

FIG. 4. Coincident particle spectra for ^{50}Ti at a scattering angle of 120° and $E_p = 11$ MeV. TAC windows were set around the true peak (upper part) and the accidental region (lower part).

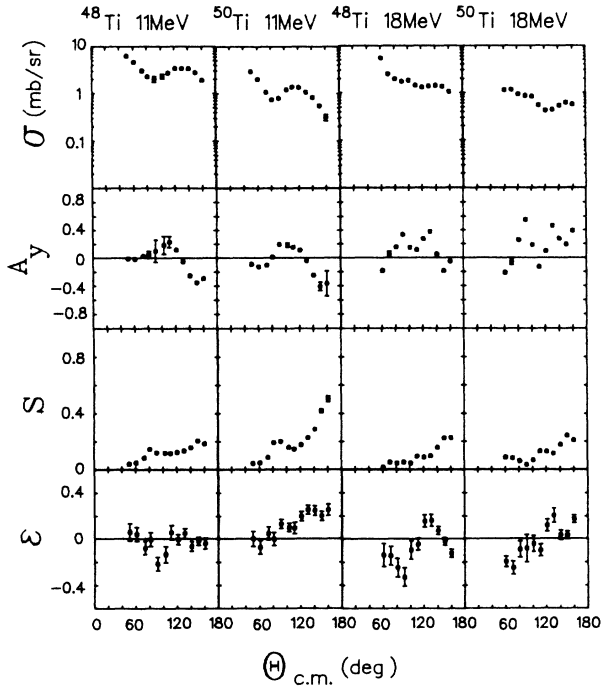

FIG. 5. Measured angular distributions of the cross section $\sigma(\theta)$, analyzing power $A_y(\theta)$, spin-flip probability $S(\theta)$, and spin-flip asymmetry $\epsilon(\theta)$.

scattering angles where the errors were comparable to the statistical errors.[10]

Characteristic features of the measured observables are as follows.

(1) The spin-flip asymmetry $\epsilon(\theta)$ has fairly large values for the ^{48}Ti and ^{50}Ti targets at $E_p = 11$ and 18 MeV.

(2) The angular distributions of the spin-flip asymmetry $\epsilon(\theta)$ has strong energy and mass-number dependence compared with the other observables.

(3) Partial differential cross sections of the spin-flip [$\sigma_{+-}(\theta)$ and $\sigma_{-+}(\theta)$] have nearly constant angular distributions whereas the cross sections of non-spin-flip [$\sigma_{++}(\theta)$ and $\sigma_{--}(\theta)$] have large forward peaks. The magnitudes of $\sigma_{+-}(\theta)$ and $\sigma_{-+}(\theta)$ are comparable with those of $\sigma_{++}(\theta)$ and $\sigma_{--}(\theta)$ at the backward angles.

IV. ANALYSES AND DISCUSSION

A. Macroscopic analyses

The macroscopic analyses based on a vibrational model were performed in terms of the coupled-channels method.[12] The optical potential used for the incident and exit channels has the standard form

$$U(r) = -V_0 f(r,r_0,a_0) + 4ia_I W_I \frac{d}{dr} f(r,r_I,a_I) + \boldsymbol{\sigma}\cdot\mathbf{L}\left[\frac{\hbar}{m_\pi c}\right]^2 \frac{V_{SO}}{r}\frac{d}{dr} f(r,r_{SO},a_{SO}) + V_C(r) \, . \tag{8}$$

The function $f(r,r_i,a_i)$ has a Woods-Saxon form

$$f(r,r_i,a_i) = \frac{1}{1+\exp[(r-R_i)/a_i]} \, , \tag{9}$$

where A is the mass number of the target, and $R_i = r_i A^{1/3}$. The potential $V_C(r)$ is the Coulomb potential due to a uniformly charged sphere with a radius of $r_C = 1.25 A^{1/3}$ fm.

The collective model form factors are obtained by deforming the optical potential. When the deformation from a sphere is represented by $\alpha_i(\hat{\mathbf{r}})$, the deformed potential $\Delta U(r)$ is written

$$\Delta U(r) = \Delta U_0(r) + \Delta U_I(r) + \Delta U_{SO}(r) + \Delta U_C(r) \, , \tag{10}$$

where

$$\Delta U_0 = -\alpha_0(\hat{\mathbf{r}}) V_0 \frac{d}{dr} f(r,r_0,a_0) \, ,$$

$$\Delta U_I = 4i\alpha_I(\hat{\mathbf{r}}) a_I W_I \frac{d}{dr}\frac{\partial}{\partial r_I} f(r,r_I,a_I) \, , \tag{11}$$

$$\Delta U_{SO} = \left[\frac{\hbar}{m_\pi c}\right]^2 V_{SO}\left[\alpha_{SO}(\hat{\mathbf{r}})\frac{1}{r}\frac{d}{dr}\frac{\partial}{\partial r_{SO}} f(r,r_{SO},a_{SO})\boldsymbol{\sigma}\cdot\mathbf{L} + \boldsymbol{\sigma}\cdot\nabla\alpha_{SO}(\hat{\mathbf{r}})\times\frac{\nabla}{i}\right] ,$$

and $\Delta U_C(r)$ is the Coulomb deformation potential. The deformation parameter β_i is related to $\alpha_i(\hat{\mathbf{r}})$ by

$$\langle IM|\alpha_i(\hat{\mathbf{r}})|00\rangle=\beta_i R_i Y_I^{M*}(\hat{\mathbf{r}})(I+1)^{-1/2} ,$$

where $|IM\rangle$ and $|00\rangle$ are the initial and final nuclear states, respectively.

The parameters of the optical potential were determined by searching the best-fit parameters automatically by use of the coupled-channels code ECIS.[13] The starting values of the optical potential parameters were taken from the parameters of Becchetti and Greenlees (BG).[14] All of the nine parameters were searched to give best fits to the experimental cross section and analyzing power of the elastic scattering. The deformation parameter β_2 was fixed to the values obtained from the Coulomb-excitation experiments: $\beta_2=0.265$ and 0.175 for ^{48}Ti and ^{50}Ti, respectively.[15] The searched optical potential parameters are given in Table I. The obtained parameters are reasonable except for the spin-orbit potential radii r_{SO}: they are smaller than the BG parameters.

The differential cross section $\sigma(\theta)$, analyzing power $A_y(\theta)$, spin-flip probability $S(\theta)$, and spin-flip asymmetry $\epsilon(\theta)$ in the excitation of the first 2^+ states in ^{48}Ti and ^{50}Ti at $E_p=11$ and 18 MeV were calculated in terms of the coupled-channels method by using the best-fit parameters listed in Table I; see Fig. 7. The deformation parameters β for the real, imaginary, and Coulomb deformations were fixed to the values obtained from the Coulomb-excitation experiments. Three values of the spin-orbit deformation parameter, $\beta_{SO}=0$, β, and 2β were examined so as to see the effect of the strength of the spin-orbit deformation to the observables. The magnitude of $\sigma(\theta)$ for both ^{48}Ti and ^{50}Ti are well reproduced by using the defor-

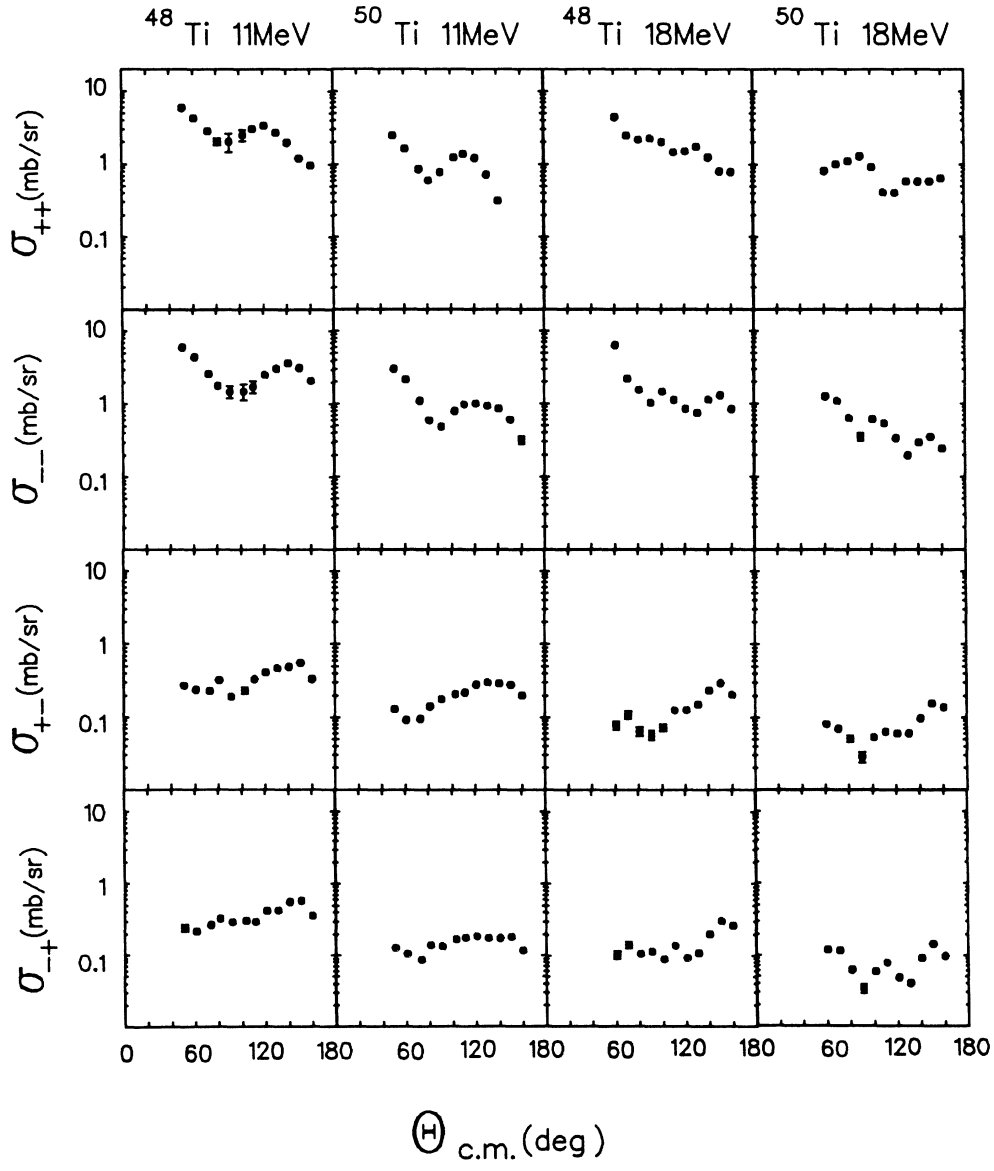

FIG. 6. Measured angular distributions of the partial cross sections.

TABLE I. Optical potential parameters used in the coupled-channels calculation. Incident energies and well depths are in MeV, and lengths are in fm.

Target	E_p	V_0	W_I	V_{SO}	r_0	r_I	r_{SO}	a_0	a_I	a_{SO}
^{48}Ti	11	52.1	8.28	5.60	1.24	1.33	0.87	0.61	0.47	0.63
^{50}Ti	11	52.1	7.56	5.74	1.21	1.31	0.82	0.60	0.60	0.60
^{48}Ti	18	58.8	8.62	6.24	1.12	1.27	0.97	0.76	0.60	0.56
^{50}Ti	18	56.9	7.79	6.94	1.13	1.15	0.93	0.70	0.74	0.66

mation parameter obtained from the Coulomb-excitation at both 11 and 18 MeV. The angular distributions of $\sigma(\theta)$, $A_y(\theta)$, and $S(\theta)$ are roughly reproduced in these calculations. The effect due to the strength of the spin-orbit deformation is negligibly small for $\sigma(\theta)$, $A_y(\theta)$, and $S(\theta)$. So the spin-dependent observables, $A_y(\theta)$ and $S(\theta)$ are mainly generated from the spin-dependent part (spin-orbit force) in the optical potential for the incident or exit channel. The calculated $\epsilon(\theta)$ is more sensitive to the strength of the spin-orbit deformation parameter β_{SO} than the $A_y(\theta)$ and $S(\theta)$ are. However, predicted $\epsilon(\theta)$ is insensitive to the incident energy and target nucleus.

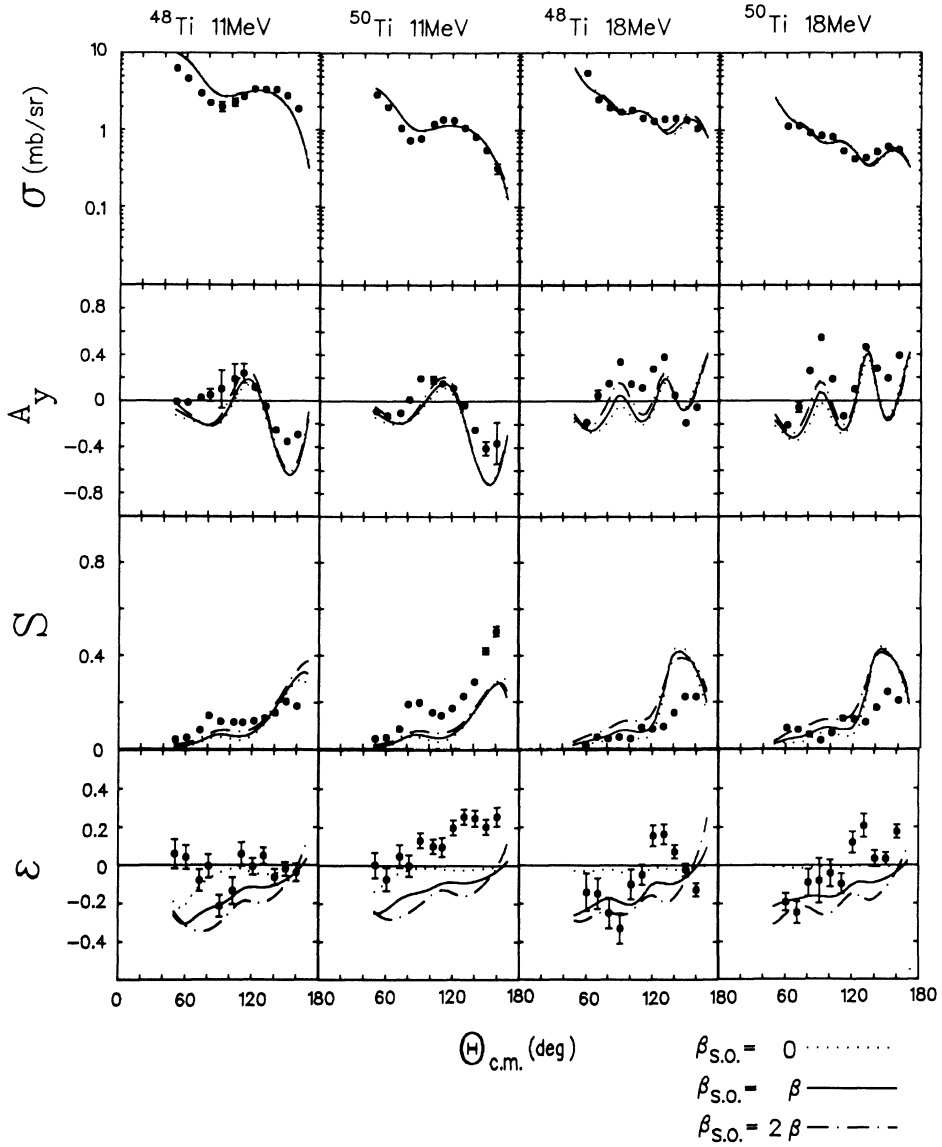

FIG. 7. Collective-model predictions of $\sigma(\theta)$, $A_y(\theta)$, $S(\theta)$, and $\epsilon(\theta)$ in the inelastic scattering to 2_1^+ state with the optical parameters of Table I. The strength of the spin-orbit deformation was varied as $\beta_{SO}=0$, β, and 2β.

B. Microscopic analyses

The active nucleons in the inelastic excitation process were assumed to be in the proton and neutron shells of $f_{7/2}$, $f_{5/2}$, $p_{3/2}$, and $p_{1/2}$. For the projectile-target interaction, a simplified nucleon-nucleon interaction which includes a spin-independent term and a spin-spin term was used in our microscopic calculation.[16] The interaction is written as

$$V(r)=(V_0+V_1\sigma_1\cdot\sigma_2)f(r)\ , \tag{12}$$

where $f(r)$ is assumed to be of Yukawa form with a range of 1 fm, and V_0 and V_1 are the strength of the spin-independent and spin-spin interactions, respectively. The nuclear-structure wave functions of ^{48}Ti and ^{50}Ti were obtained from the shell-model calculation by Ogawa.[17] The modified Kuo-Brown matrix elements[18] were adopted as the two-body effective interaction. The configuration space spanned is

$$(0f_{7/2})^n+(0f_{7/2})^{n-1}(1p_{3/2},0f_{5/2},1p_{1/2})^1 +(0f_{7/2})^{n-2}(1p_{3/2},0f_{5/2},1p_{1/2})^2\ .$$

The number of active particles is $n=A-40$, where A is the mass number of the target nuclei ^{48}Ti and ^{50}Ti. The spectroscopic amplitudes (one-body transition density) derived from the calculation are shown in Table II. The main contribution of the single-particle transition elements to the inelastic scattering is the $0f_{7/2}\rightarrow 0f_{7/2}$ proton transition for ^{50}Ti and the $0f_{7/2}\rightarrow 0f_{7/2}$ transition of both proton and neutron for ^{48}Ti.

The inelastic scattering observables were calculated by the computer code DWBA74[19] under the adiabatic approximation. The BG parameter set was used for the optical potential which has the form given by Eq. (8). Results of the microscopic calculations of $\sigma(\theta)$, $A_y(\theta)$, $S(\theta)$, and $\epsilon(\theta)$ for ^{48}Ti and ^{50}Ti at $E_p=18$ MeV are shown in Fig. 8, where V_0 is fixed to 100 MeV which is determined to reproduce the experimental cross sections, and the ratio of the spin-dependent and spin-independent strength are taken as $V_1/V_0=0$, $\frac{1}{8}$, and $\frac{1}{4}$ to see the effect of the spin-dependent interaction. The fit to the $A_y(\theta)$ is worse than that obtained in the collective model calculations, but the fit to the $S(\theta)$ is improved. As in the case of the previous macroscopic calculation, the $\sigma(\theta)$, $A_y(\theta)$, and $S(\theta)$ are not sensitive to the strength of the spin-dependent interaction. The predicted spin-flip asymmetry is similar to that of the collective model calculation and cannot reproduce the observed target dependence.

Zero spin-flip asymmetry is predicted when the spin-dependent part of the interaction Eq. (12) is neglected, which is consistent with the prediction by Satchler.[6] The magnitude of $\epsilon(\theta)$ is roughly reproduced only when $V_1/V_0=\frac{1}{8}$. The strength of the spin-dependent force thus obtained is smaller than that considered previously.[16,20] The calculated $\epsilon(\theta)$ have negative values for both ^{48}Ti and ^{50}Ti. Results of the calculation of $V_1/V_0=-\frac{1}{8}$ are shown in Fig. 9, together with the calculation of $V_1/V_0=+\frac{1}{8}$. The opposite sign in the ratio V_1/V_0 generates the sign change of the calculated spin-flip asymmetry. The reason is clearly understood because the interference term, which is the numerator of Eq. (7), changes the sign. The result clearly demonstrates that the spin-flip asymmetry $\epsilon(\theta)$ is sensitive to the relative sign of the spin-independent and spin-dependent interactions as well as the strength of the spin-dependent interaction.

TABLE II. Spectroscopic amplitudes (one-body transition density) between 0_g^+ and 2_1^+ states of ^{48}Ti and ^{50}Ti obtained from shell-model calculation.

One-body	^{48}Ti		^{50}Ti	
transition density	Proton	Neutron	Proton	Neutron
$D(f_{7/2},f_{7/2})$	−0.340	−0.593	0.630	−0.002
$D(f_{7/2},p_{3/2})$	−0.194	−0.287	0.122	0.369
$D(f_{7/2},f_{5/2})$	−0.023	−0.193	0.013	0.159
$D(p_{3/2},p_{3/2})$	−0.018	−0.037	0.010	0.018
$D(p_{3/2},f_{5/2})$	−0.013	−0.023	0.010	0.010
$D(f_{5/2},f_{5/2})$	−0.004	−0.013	0.007	0.023
$D(f_{5/2},p_{1/2})$	−0.009	−0.022	0.014	0.020

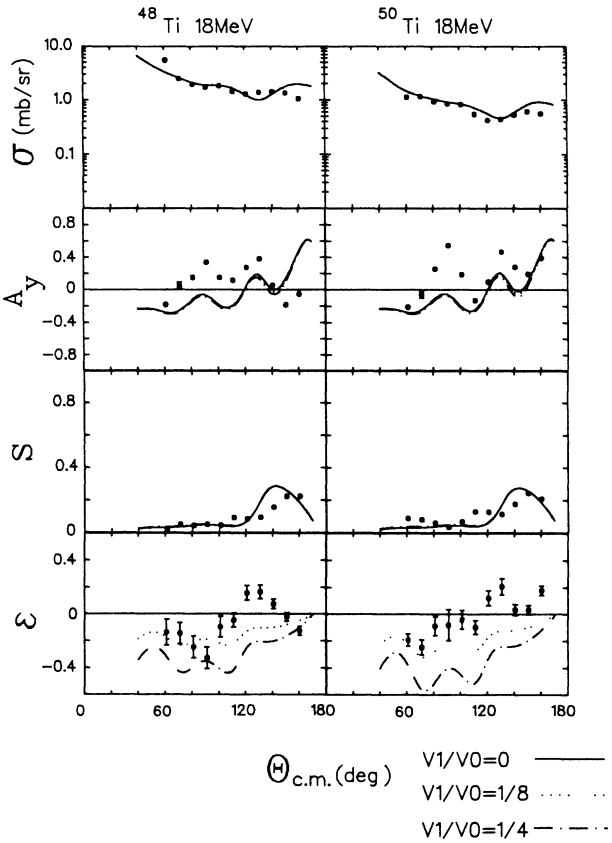

FIG. 8. Microscopic calculations of $\sigma(\theta)$, $A_y(\theta)$, $S(\theta)$, and $\epsilon(\theta)$. The strength of the spin-independent force is fixed at 100 MeV, and that of the spin-spin interaction was varied as $V_1/V_0=0$, $\frac{1}{8}$, and $\frac{1}{4}$.

Next the isospin-dependent interaction was taken into account as[12]

$$V(r)=\{V_{00}+V_{01}(\tau_1\cdot\tau_2)+[V_{10}+V_{11}(\tau_1\cdot\tau_2)]\sigma_1\cdot\sigma_2\}f(r)\ , \quad (13)$$

where $f(r)$ is assumed to be Yukawa form with a range of 1 fm as before. The term V_{ST} gives rise to a spin transfer of S and an isospin transfer of T. From Eq. (13) the proton-neutron interaction is written as

$$V_{pn}=[(V_{00}-V_{01})+(V_{10}-V_{11})\sigma_1\cdot\sigma_2]f(r)\ , \quad (14)$$

and the proton-proton interaction is

$$V_{pp}=[(V_{00}+V_{01})+(V_{10}+V_{11})\sigma_1\cdot\sigma_2]f(r)\ . \quad (15)$$

The relative strength of the spin-independent and -dependent term in Eq. (12) for the proton-neutron interaction is

$$V_0=V_{00}-V_{01}=11\ ,$$

and

$$V_1=V_{10}-V_{11}\equiv 1\ .$$

For the proton-proton interaction, we have

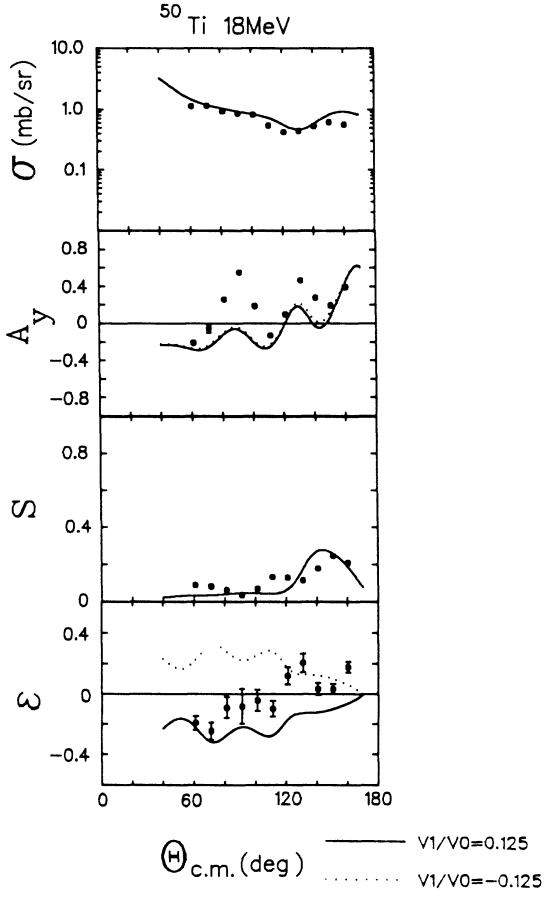

FIG. 9. Comparison of the calculations with $V_1/V_0=+\frac{1}{8}$ and $-\frac{1}{8}$.

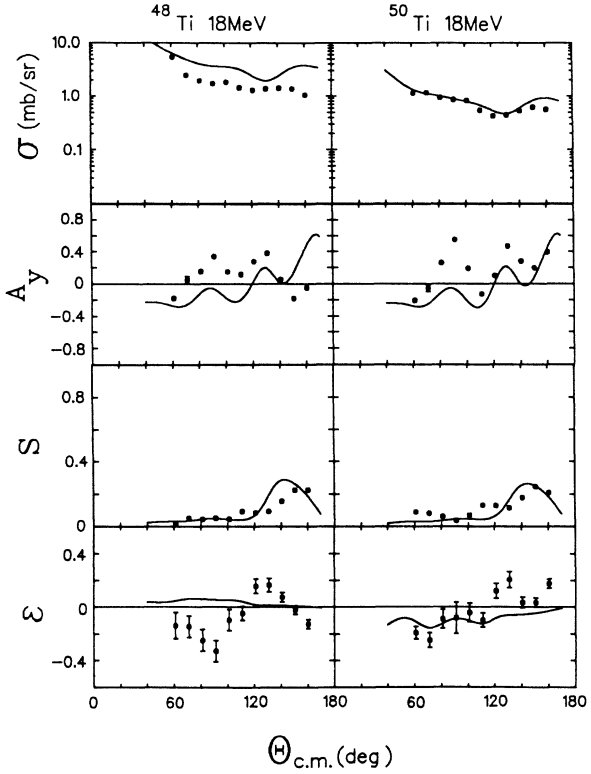

FIG. 10. The effect of the isospin-dependent interaction to the observables.

$$V_0=V_{00}+V_{01}=4\ ,$$

and

$$V_1=V_{10}+V_{11}=-4\ ,$$

in units of the strength of the spin-dependent term for the proton-neutron interaction.[21] The numerical calculations were done by using the computer code DWBA74 with the BG optical potential parameter set and employing the adiabatic approximation. The strength of the interaction used in the calculations was determined to reproduce the experimental cross sections. The calculations for ^{48}Ti and ^{50}Ti at 18 MeV are shown in Fig. 10. The effect of the isospin-dependent interaction is quite small for $\sigma(\theta)$, $A_y(\theta)$, and $S(\theta)$. But the predicted $\epsilon(\theta)$ is sensitive to the isospin-dependent interaction, which causes a large difference between ^{48}Ti and ^{50}Ti. Such a target dependence arises from the different contributions in proton-proton and proton-neutron interaction parts between ^{48}Ti and ^{50}Ti because of the difference in the microscopic nuclear structure.

V. CONCLUSION

The angular distributions of four independent observables—differential cross section, analyzing power, spin-flip probability, and spin-flip asymmetry—in the excitation of the first 2^+ in ^{48}Ti and ^{50}Ti have been mea-

sured at 11 and 18 MeV using the $(p,p'\gamma)$ coincidence technique with the polarized beam. This is the first measurement of spin-flip asymmetry done to study the direct reaction mechanism. The spin-flip asymmetry has fairly large values for the ^{48}Ti and ^{50}Ti targets at 11 and 18 MeV. A strong energy dependence and mass-number dependence were observed in the spin-flip asymmetry.

The data were compared with both the macroscopic coupled-channels calculation on the vibrational model and the microscopic DWBA calculation. The macroscopic analysis represents that the $\epsilon(\theta)$ is more sensitive to the strength of the spin-orbit deformation parameter β_{SO} than the $A_y(\theta)$ and $S(\theta)$ are. But predicted spin-flip asymmetry is insensitive to incident energy and target nucleus. The microscopic DWBA using the shell-model wave functions derived from the modified Kuo-Brown interactions with the simplified effective interaction predicted a small contribution of the spin-dependent interaction to $\sigma(\theta)$, $A_y(\theta)$, and $S(\theta)$, but $\epsilon(\theta)$ is sensitive to the strength of the spin-dependent interaction, just like the macroscopic calculation was. The effect of the isospin-dependent interaction is quite small for $\sigma(\theta)$, $A_y(\theta)$, and $S(\theta)$. On the other hand, the predicted $\epsilon(\theta)$ is sensitive to the isospin-dependent interaction, which causes a large difference between ^{48}Ti and ^{50}Ti. This comes from the different contributions of proton-proton and proton-neutron interaction parts between ^{48}Ti and ^{50}Ti because of the difference of the microscopic nuclear structure. Further systematic experiments and analyses are necessary to (1) obtain a quantitative fit between the data and the calculation and (2) investigate the relation between the spin-flip asymmetry and the nuclear structure involved.

ACKNOWLEDGMENTS

We would like to thank Dr. K. Ogawa for the calculations of the wave functions. We also acknowledge the help and cooperation of Mr. Y. Kondo and Mr. M. Tsunoda, and the Tandem Accelerator Center staff.

*Present address: Department of Physics, Tokyo University of Mercantile Marine, Koto-ku, Tokyo 135, Japan.

[1]C. Glashausser, R. de Swiniarski, J. Thirion, and A. D. Hill, Phys. Rev. **164**, 1437 (1967).

[2]F. H. Schmit, R. E. Brown, J. B. Gerhart, and W. A. Kolasinski, Nucl. Phys. **52**, 353 (1964).

[3]R. N. Boyd, D. Slater, R. Arida, H. F. Glavish, C. Glashausser, G. Bissinger, S. Davis, C. F. Haynes, and A. B. Robbins, Phys. Rev. Lett. **29**, 955 (1972).

[4]J. H. Feist, W. Kretschmer, P. Pröschel, and G. Graw, Nucl. Phys. **A290**, 141 (1977).

[5]T. Fujisawa, N. Kishida, T. Kubo, T. Wada, Y. Toba, T. Hasegawa, M. Sekiguchi, N. Ueda, M. Yasue, F. Soga, H. Kamitsubo, M. Nakamura, K. Hatanaka, Y. Wakuta, T. Tanaka, and A. Nagao, J. Phys. Soc. Jpn. **50**, 3198 (1981).

[6]G. R. Satchler, Phys. Lett. **19**, 312 (1965).

[7]H. Sherif, Can. J. Phys. **49**, 983 (1971).

[8]T. Fujisawa, Ph.D. thesis, Osaka University, 1982.

[9]Y. Tagishi and J. Sanada, Nucl. Instrum. Methods **164**, 411 (1979).

[10]T. Murayama, H. Sakamoto, M. Oyaizu, Y. Tagishi, and S. Seki, J. Phys. Soc. Jpn. Suppl. **55**, 1118 (1986).

[11]Y. Tagishi, T. Sakai, M. Tomizawa, H. Nishikawa, S. Hiroki, and A. Kurashima, Annual Report UTTAC-54, 1988.

[12]G. R. Satchler, *Direct Nuclear Reactions* (Clarendon, Oxford, 1983).

[13]J. Raynal, computer code ECIS (unpublished).

[14]F. D. Becchetti, Jr. and G. W. Greenlees, Phys. Rev. **182**, 1190 (1969).

[15]P. H. Stelson and L. Grodzins, Nucl. Data Tables **A1**, 21 (1965).

[16]G. R. Satchler, Nucl. Phys. **A95**, 1 (1967).

[17]H. Miyatake, K. Ogawa, T. Shinozuka, and M. Fujioka, Nucl. Phys. **A470**, 328 (1987).

[18]T. T. S. Kuo and G. E. Brown, Nucl. Phys. **A114**, 241 (1968).

[19]J. Raynal, computer code DWBA74 (unpublished).

[20]D. L. Hendrie, C. Glashausser, J. M. Moss, and J. Thirion, Phys. Rev. **186**, 1188 (1969).

[21]N. K. Glendenning and M. Veneroni, Phys. Rev. **144**, 834 (1965).